Non-destructive characterisation of dolerite archaeological artefacts

Mirco Ramacciotti [a,b], Gianni Gallello [a,*], Joaquin Jiménez-Puerto [a], Joan Bernabeu [a], Teresa Orozco Köhler [a], Sonia Rubio-Barberá [b], Agustín Pastor [b]

[a] Department of Prehistory, Archaeology and Ancient History, University of Valencia, Avenida de Blasco Ibáñez 28, 46010 Valencia, Spain
[b] Analytical Chemistry Department, University of Valencia, Edifici Jeroni Muñoz, Dr. Moliner 50, 46100 Burjassot, Spain

ARTICLE INFO

ABSTRACT

A methodological proposal for the characterisation of dolerite rock aiming to test a non-destructive and non-invasive analytical approach has been developed. Geological samples were collected from several natural outcrops and studied together with seven archaeological stone tools found in a Chalcolithic site of the southern Valencian Community (Spain). The samples were analysed employing portable energy dispersive X-ray fluorescence spectroscopy, Raman microspectroscopy and Fourier transform near infrared spectroscopy. The obtained data were statistically processed in order to evaluate affinities and differences among the geological outcrops and to evaluate the possible provenance of the stone tools. The results of the different techniques were compared and evaluated. The three techniques showed results that were in most of the cases consistent one with each other, suggesting that combining multielement analysis and Raman could be a good way to identify stone tools raw material procurement, being the prior step for the reconstruction of ancient exchange networks.

1. Introduction

This study is developed within the framework of NEONETS[1] project, whose general aim is the identification of raw material outcrops in the Mediterranean region of the Iberian Peninsula in order to analyse the polished stone tools exchange networks between the Neolithic and the Bronze Age, a common element in these chronological contexts.

The use of chemical methods is widely asserted for provenance study of archaeological lithic objects. Indeed, the characterisation of samples collected from natural outcrops, and artefacts found during archaeological excavations and field surveys permits to link the stone tools to potential raw material sources, developing provenance hypotheses which rely on more robust and objective data than those obtained only by a naked-eye examination [1–4].

Several techniques have been used for this purpose. Energy dispersive X-ray fluorescence spectroscopy (ED-XRF) and inductively coupled plasma mass spectrometry (ICP-MS) have been used in several studies to perform multielement analysis [5–9]. On the other hand, X-ray diffraction (XRD) and Fourier transform infrared spectroscopy (FT-IR) [10–11] are frequently employed to determine the main mineralogical phases present in the studied rocks. Furthermore, in the last few years, researchers are relying more and more on non-invasive techniques, since

in most cases the archaeological materials cannot be damaged, often employing portable equipment which can be used in museum or in-field such as portable ED-XRF devices (pED-XRF) [12–14].

The aim of the work is to compare the results obtained by three different non-destructive techniques in order to evaluate, cross-reference and discuss the obtained information. Dolerite artefacts found in the Chalcolithic Age settlement of Sanxo Llop (Gandia, Valencian Community, Spain) and potential raw materials from different natural outcrops (Fig. 1) were characterised from the chemical point of view employing pED-XRF, Raman microspectroscopy and FT-NIR, and multivariate statistics and elemental correlations were used to explore the obtained results to identify the possible provenance of the studied materials.

Dolerite is one of the lithotypes used by prehistoric populations to make stone tools. Also known as diabase, it is a medium grained mafic rock characterised by an ophitic texture and composed of calcic plagioclases and clinopyroxenes (mainly augite), and lower amounts of other minerals such as olivine, orthopyroxenes (especially enstatite), felspathoids, opaque minerals and quartz, as well as secondary clay minerals and amphiboles [15]. Several archaeometric works deal with the analysis and characterisation of dolerite of archaeological interest [12,16–18]. In particular, destructive analytical methods have been

---

employed in the last two decades to investigate the origin of doleritic bluestones linked to the archaeological site of Stonehenge [19–20], and, in the last few years, Bevins and colleagues rediscussed the issue employing a different approach based on compatible element geochemistry and principal component analysis, and, more recently, on rare earth elements (REE) as provenance markers [21]. The identification and characterisation of the dolerite outcrops in the Valencian Community employed as raw material sources was carried out by Orozco Köhler [22]. Furthermore, the rocks from the selected outcrops were previously analysed by multielement analysis and, for the first time, Gallello and colleagues tested the effectiveness of REE and REE fractionation parameters as markers to discriminate among potential sources of dolerite and retrace the origin of rocks from archaeological contexts [23–24].

2. Materials and methods

2.1. Sampling

Samples and their provenance are resumed in the Table 1.

The sampling comprehends several fragments of dolerite collected from different potential quarries mainly located in the southern Valencian Community (Fig. 1; M1: Pinoso-Xirnolet, PX; M6: Sierra Orihuela, SO; M7: Finestrat, FIN; M14: Vinalopó, VIN), although M2 comes from Altura (ALT), in the province of Castellón, and M12 and M21 from Almansa (ALM) in the province of Albacete (Castilla-La Mancha). Finally, seven archaeological artefacts were chosen to perform the analysis (S1-S7), which come from the archaeological Chalcolithic Age settlement excavated in Sanxo Llop (SL; Gandía, Valencia).

2.2. Portable energy dispersive X-ray fluorescence spectroscopy (pED-XRF)

The multielement analysis was carried out directly on different

Table 1
Samples and their origin.

Sample	Type	Origin	Outcrop Code
M1	Geological	Pinoso-Xirnolet	PX
M2	Geological	Altura	ALT
M6	Geological	Sierra Orihuela	SO
M7	Geological	Finestrat	FIN
M12	Geological	Almansa	ALM
M21	Geological	Almansa	ALM
M14	Geological	Vinalopó	VIN
S1	Archaeological	Sanxo Llop	SL
S2	Archaeological	Sanxo Llop	SL
S3	Archaeological	Sanxo Llop	SL
S4	Archaeological	Sanxo Llop	SL
S5	Archaeological	Sanxo Llop	SL
S6	Archaeological	Sanxo Llop	SL
S7	Archaeological	Sanxo Llop	SL

surface points of the samples using a hand-held S1 Titan pED-XRF by Bruker (Kennewick, Washington, USA) equipped with a Rh X-ray tube (50 kV) and a X-Flash silicon drift detector (resolution: 147 eV; FWHM: 5.9 keV). Geochem-trace application was used to perform the quantitative analysis of Al, Si, K, Ca, Ti, Fe, Zn, Rb, Sr, Y, Zr and Ba concentrations of all the geological and archaeological samples.

2.3. Raman microspectroscopy

The analyses were carried out employing a XploRA Raman emission spectrometer coupled to a confocal microscope by Horiba MTB. Laser wavelength was 785 nm and the measurements were characterised by an acquisition time of 5 s and 5 accumulations.

Two up to four areas were selected in the samples and in each area several measurement spots were randomly chosen for the analysis and the spectra were averaged. The region between 220 and 1100 cm^{-1} was taken into account.

Fig. 1. Localisation of the sampled dolerite outcrops (ALM: Almansa, ALT: Altura, FIN: Finestrat, PX: Pinoso-Xirnolet, SO: Sierra Orihuela, VIN: Vinalopó) and the site of provenance of the studied archaeological materials (Sanxo Llop: SL).

All the archaeological and geological samples were analysed by Raman microspectroscopy.

2.4. Fourier transform near infrared spectroscopy (FT-NIR)

In order to obtain the NIR spectra of the samples, a MPA model Multipurpose Analyzer FT-NIR spectrometer by Bruker (Ettlingen, Germany) was employed, equipped with an integrating sphere and a fibre optic probe used for diffuse reflectance spectra acquisition. The OPUS software 6.5 from Bruker was employed for instrument controlling and data acquisition. Both archaeological and geological samples were analysed in different surface points using a fibre optic probe. The resolution was 4 cm^{-1} and each spectrum, recorded in Kubelka–Munk units, is the average of 50 cumulating scans in the 14,000–4000 cm^{-1} region. Each point was analysed three times with these parameters and the three measurements were finally averaged. The background was obtained from the closed integrating sphere using the above-quoted instrumental conditions. The samples analysed by FT-NIR are S1-7 (archaeological materials), M1 (PX), M6 (SO), M7 (FIN), M12 (ALM), M14 (VIN) (geological materials).

2.5. Data analysis

Data analysis was carried out through R (version: 4.1.2) [25]. Principal component analysis (PCA) was used to explore the results obtained on geological samples through the three techniques in order to evaluate the role of the variables in complex datasets. Scores of archaeological samples for Raman and FT-NIR analyses were subsequently predicted in geological samples models, and cluster analyses with PCA scores (variables: PC1 to PC3) was performed to evaluate the possible provenance of the artefacts using complete linkage clustering method. Kohonen networks or Self Organised Maps (SOM) were also used on pED-XRF, Raman

and FT-NIR data of geologic samples. The self-organized topological feature maps [26] are a specific concept to deal with multidimensional non-linear representations and map them in a two-dimensional space of neurons. SOM work through the premise of mapping the input so that similar signals excite spatially close neurons [27], following an unsupervised learning protocol. As previous works have pointed out, SOM are reasonably tolerant to noise and enable the discovery of hidden patterns in a more efficient way than PCA [28]. Ggplot2 (version: 3.3.5) [29], plotly (version: 4.10.0) [30] and kohonen (version: 3.0.11) [31] R packages were employed. Finally, Sr, Ba and Rb were identified as discriminant elements, therefore scatterplots of Sr vs Ba and Sr vs Rb were employed to observe natural and archaeological materials distribution.

3. Results

3.1. Multielement analysis results

Results of pED-XRF analyses are reported in the Supplementary Online Materials (Annex 1a).

Exploratory data analysis was carried out by PCA on the natural samples employing all the elemental concentrations as variables (Fig. 2).

Samples/scores plot (Fig. 2a) shows that the sample from ALT can be distinguished from the others on PC1 due to the very low scores caused by high concentrations of most of the elements, as suggested by PC1 loadings (Fig. 2b). On the other hand, VIN sample can be distinguished on PC2 axis, although some points fall with the other natural samples. This sample is characterised by very high levels of Ba and Sr, which have the most intense negative loadings for PC2 (Fig. 2b). No clear tendencies can be observed on PC3 (Fig. 2a).

Furthermore, XRF samples have been mapped with SOM and four clusters were created (see Fig. 3 and Supplementary Online Materials:
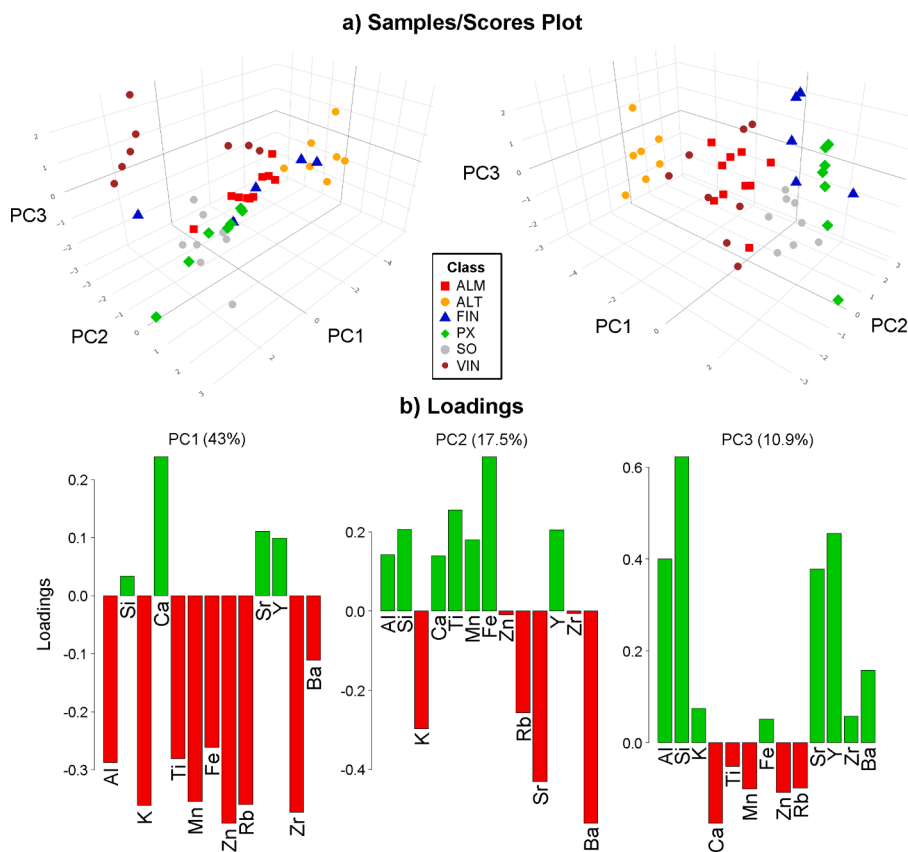

Fig. 2. PCA of natural samples: (a) samples/scores plot and variables/loadings plots for PC1, PC2 and PC3 (b).
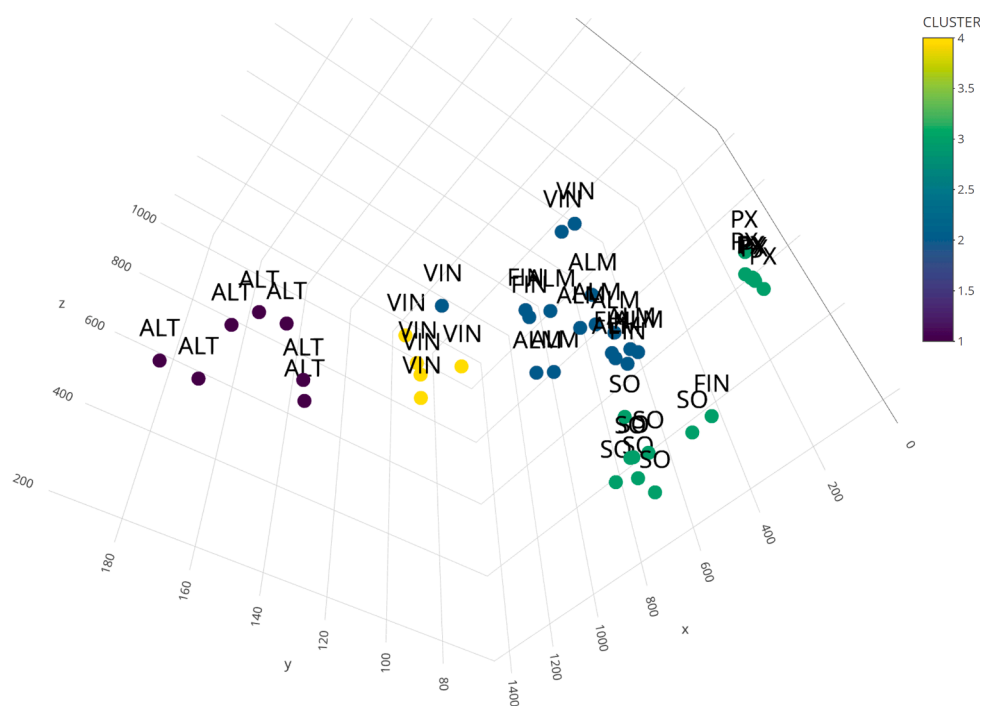
Fig. 3. Clustering map for SOM of pED-XRF data in which the original source of the sample has been added. The colours represent the SOM cluster in which they are mapped. https://zenodo.org/record/7193712/files/image.html?download=1.

Annex 1b). The results were quite similar to those provided by the PCA and they seem to group reasonably well the raw material sources. Nevertheless, a bigger sample would be needed in order to obtain more conclusive results.

Anyway, the interpretation of elemental concentrations obtained by pED-XRF analysis carried out directly on rock samples for provenance

Table 2

Main identified bands of the average spectra from geological samples and artefacts.

Mineral	Wavenumber (cm^{-1}, reference)	PX	ALT	SO	FIN	ALM	VIN	S1	S2	S3	S4	S5	S6	S7
Olivine/Clay	242 [37]/245 [38]		245			250	247	250	250	250	255	250	250	260
Plagioclase	267–281 [39]	272	275	275	270	270		274			272	270	270	
Chalcopyrite	293 [40]						298							
Clinopyroxene/Magnetite	304–327 [35]/301 [41]	315	316	305	305	308		310	315	315	310	308	308	312
Orthopyroxene/Chalcopyrite	344 [42]/352 [40]						348							
Clinopyroxene	360 [35]	360	360	360	363	365		365	368	368	365	365	365	363
Chalcopyrite	378 [40]						378							
Orthopyroxene/Nepheline/Apatite	422 [42]/426 [43]/430 [44]	418	415	417	420	422	423	420	425	425	420	420	422	425
Apatite/Quartz	447–450 [44]/462 [45]	470	460		450									
Plagioclase	485 + 505 [46]	498	500	492	497	498	486	500	495	495	495	495	495	500
Magnetite	538 [47]	545	540	545	545	545	538				545			
Clinopyroxene/Chlorite	533–555 [48]/552 [49]	560		560	560	560		545	560	560	560	550	550	550
Apatite/Titanite	591 + 607 [44]/606 [41]	610	600	605	610	605		598	593	590	610	605	600	610
Clinopyroxene/Orthopyroxene/ Magnetite/Hornblende	660 [50]/664 [42]/666 [41]	655	665	656	656	656		656	660	660	655	655	657	660
Chlorite/Serpentine	683/690 [49]								685	685	685	685	685	
Chromite	705 [41]						698							
Plagioclase	741–772 [36]	740 760	745	745	735 760	750	730 760 775	745	745	745	755	750	750	750
Olivine	817 [37]	810	810	823	810	823		816	815	815	815	815	810	810
Olivine	840 [37]	840	840	840	840	840	845	840	840	840	840	840	840	840
Clinopyroxene	863 [48]	870	870	870	870	870		870	870	870	870	870	870	870
Clinopyroxene	900 [51]	895	895	885	895	890	895	895	885	885	895	890	890	895
Apatite	956 [45]	950	950	940	945	950		950	947	950	945	950	947	947
Clinopyroxene/Orthopyroxene	1006 [48]/1013 [42]	1003			1005	1003		1003			1005	1005	1005	1005
Orthopyroxene/Clinopyroxene	1013–1035 [42]/1038 [35]	1038	1027	1038	1038	1038	1030	1035	1035	1035	1045	1035	1037	1045
Carbonates	~1080 [52]	1080		1080					1075	1075	1075			

studies must be carefully revised due to surface weathering and contamination problems, as well as to the limitations of the technique. The selection of the appropriate provenance markers is firstly linked to the studied lithotype, since elements behaviour is determined by rock mineralogy [19]. Concerning dolerite and other igneous rocks, previous works [19,32–33] pointed out the reliability of some trace elements among the ones analysed in the present work, such as Sr, Zr, Ba and Rb, while lighter elements (Si, Al, Ca), as well as Fe and Mn, are often disregarded since the analytical results are affected both by weathering and surface contamination, and by problems related to the low critical penetration depth, which limits the results to the very surface of the studied dolerite. Potts et al. [32] did not find any significant difference for Ti and Zn concentrations between weathered and not-weathered surfaces. However, Ogburn et al. [33] found an enrichment of these two elements in weathered samples, and, though it is often considered a less mobile element, William-Thorpe and colleagues [19] suggested caution for Ti results due to the low critical penetration depth. Y concentrations are usually close to the limits of detection [34] therefore the quality of the obtained results should be verified. Concerning the concentrations of Sr, Ba, Zr, Rb (see scatterplots in Annex 1c), the sample from PX can be distinguished from the others due to the low concentrations of Ba and Rb. On the other hand, the sample from ALT has the highest levels of Zr and Rb, while VIN the highest ones of Sr.

3.2. Raman microspectroscopy results

The average Raman spectra for the different outcrops and the archaeological samples are shown in the Supplementary Online Materials (Annex 2a and Annex 2b, respectively).

Most of the spectral features (Table 2) can be attributed to dolerite essential minerals like plagioclases and clinopyroxenes but some bands could be attributed also to other minerals often encountered in this rock as well as to accessory and secondary phases [15]. Anyway, the complexity of the spectra and the possible overlapping of bands from different minerals make a precise identification difficult. Concerning peak shifts, they could be explained with differences in the chemical composition of these minerals. Indeed, bands position in clinopyroxenes is determined by the metal cations in the crystal, like Mg, Ca and Fe [34], while proportions in Ca and Na determine bands position for plagioclase ($NaAlSi_3O_8$, albite – $CaAl_2Si_2O_8$, anorthite) [36]. Similarly, the fayalite (Fe_2SiO_4) and forsterite (Mg_2SiO_4) ratio determines wavenumber and characteristics of the olivine doublet band close to 830 cm^{-1} [37]. It is worth noting that sample from VIN shows also characteristic peaks for chalcopyrite, which do not appear in the other natural samples. Archaeological samples have features similar to the geological ones. However, peaks attributable to secondary minerals like chlorite and serpentine seem to be more evident here than in geological samples, maybe due to different degrees of alteration (see the Supplementary Online Materials, Annex 2b).

Because of the number of variables to be taken into account and to the complexity of the spectra, PCA was used. The obtained data were processed by Savitzky-Golay filter (polynomial order: 3rd, points: 21, derivative: 2nd) and standard normal variate (SNV), and then mean-centred. The first two PC explain 41.1 % and 24 % of the whole variance, while PC3 explains 11.5 % of it. As can be observed in the samples/ scores plot (Fig. 4a), measurements from ALM, FIN and VIN group together, mostly characterised by positive PC1 values and scattered in both negative and positive sides of PC2-axis, although two out of three FIN points have higher PC3 scores. Geological samples from PX and SO have lower PC1 scores, compared to the other ones, while ALT is characterised by positive PC1 scores but the lowest PC2 ones. Variables/ loadings plots (Fig. 4b) show the regions of the spectra which have the
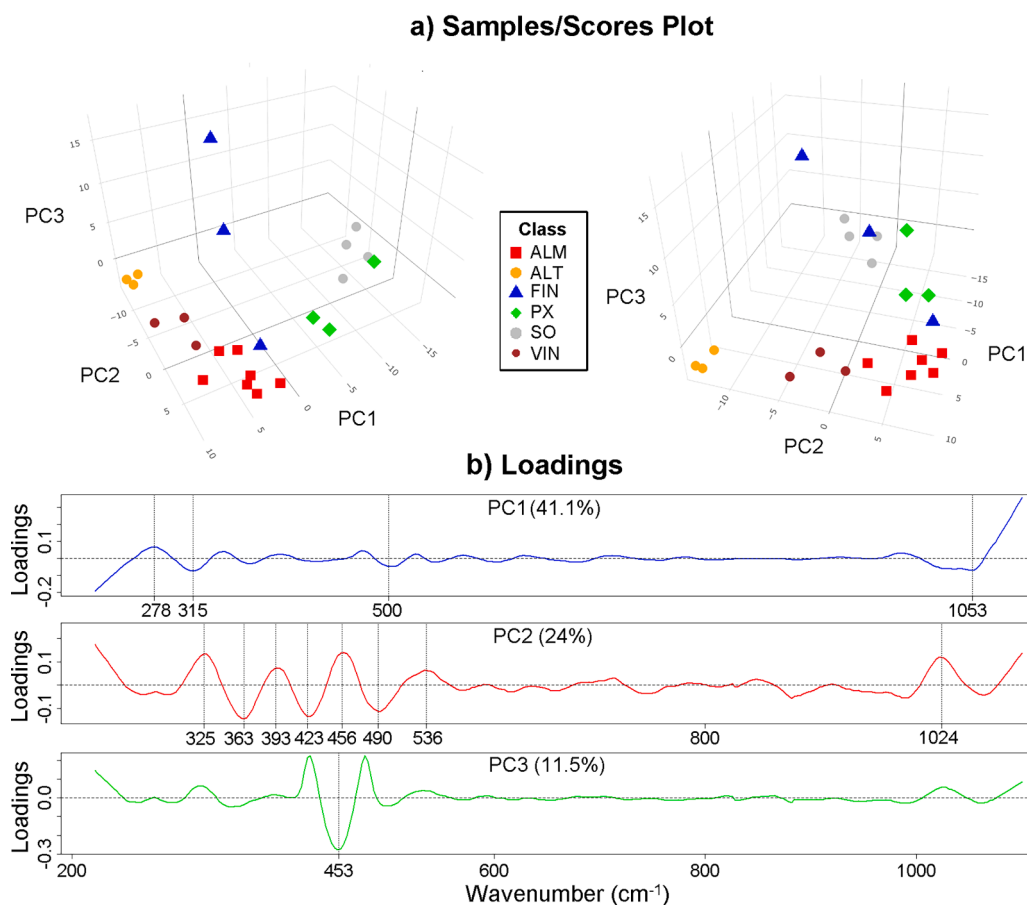
a) Samples/Scores Plot

b) Loadings

Fig. 4. PCA of Raman microspectroscopy results in geological samples: samples/scores plot (a) and variable/loadings plot for PC1, PC2 and PC3 (b).

highest influence on the model, which for both PC1 and PC2 are those mostly linked to plagioclases and pyroxenes. High PC3 scores for FIN sample are instead possibly tied on 450 cm^{-1} band, probably due to the presence of quartz. Differences in mineralogical composition could have been determined by melt characteristics and crystallisation dynamics which interested the outcropping area of the intrusive formation [15].

The use of SOM on Raman data could not clearly group the sources of raw materials (see the Supplementary Online Materials: Annex 2c-d). This uncertainty is probably produced by a conjunction of the small size of the available sample, and the large number of variables considered in the analysis. In order to enhance the results, it would be needed to increase the size of the sample substantially.

3.3. Infrared spectroscopy results

The average FT-NIR spectra in the region between 7400 and 4000 cm^{-1} for geological and archaeological dolerites are shown in the Supplementary Online Materials (Annex 3a).

Geological samples show their main features close to 7100 cm^{-1}, between ~5235 and ~5000 cm^{-1}, and between ~4530 and ~4190 cm^{-1}. The first composite band can be attributed to OH stretching vibrations, while the second and the third ones to H—O—H bends and metal-OH vibrational modes respectively [53]. These features are ascribable to hydrous phases like amphiboles or phyllosilicates [54], which can be found as accessory or minerals alteration in dolerite [55]. Concerning the most evident differences among outcrops, FIN and ALM have and intense band at ~4270 cm^{-1}, while the other samples have a peak at ~4310 cm^{-1}. ALM shows also a peak at ~4485 cm^{-1}, while PX and SO at 4530 cm^{-1}. According to Clark et al. [53], Al-OH and Fe-OH

bands occur close to 4500 cm^{-1} and to 4370 cm^{-1} respectively, and Mg-OH ones close to 4300 cm^{-1}. However, the proportion of these metals can cause band shifts and, concerning clay minerals, band position also depends on Si substitution by Al and Fe in the tetrahedral sites [54]. The artefacts have peaks close to these wavenumbers as well, although in some samples (S1, S4-7) bands are less resolved than the ones of the natural samples, maybe due to alterations phenomena or weathering, which determined different FT-NIR profiles.

In order to explore the results of FT-NIR spectroscopy and investigate about the difference among geological samples and the provenance of the archaeological ones, PCA was employed. Absorbance values between 5500 and 4100 cm^{-1} were used as variables to carry out data analysis and data were pre-processed through Savitzky-Golay filter (polynomial order: 3rd, points: 21, derivative order: 2nd) and SNV, and subsequently mean-centred. The first three PCs account for 55.7 %, 13.5 % and 11.7 % of the overall variance, respectively. Samples/scores plot for PC1 vs PC2 (Fig. 5a) shows that natural samples are divided on PC1-axis, being FIN and ALM points plotted on the positive side, while VIN, PX and SO points fall on the negative one.

Concerning PC3, ALM points are characterised by lower scores than FIN ones. Looking at the variables/loadings plots (Fig. 5b) can help in the identification of the causes of the sample distribution. It can be observed that the most intense loadings are concentrated in the region between 4530 and 4195 cm^{-1}. The highest PC1 loadings peaks are at 4350, 4315 and 4195 cm^{-1}. On the other hand, the lowest loadings are around 4250 cm^{-1}. The different scores related to the peaks at 4350, 4315 and 4250 cm^{-1} are probably linked to the intense metal-OH band in this region of the spectra, which, as previously stated, is at higher wavenumbers for PX, SO and VIN (~4310 cm^{-1}) than for ALM and FIN
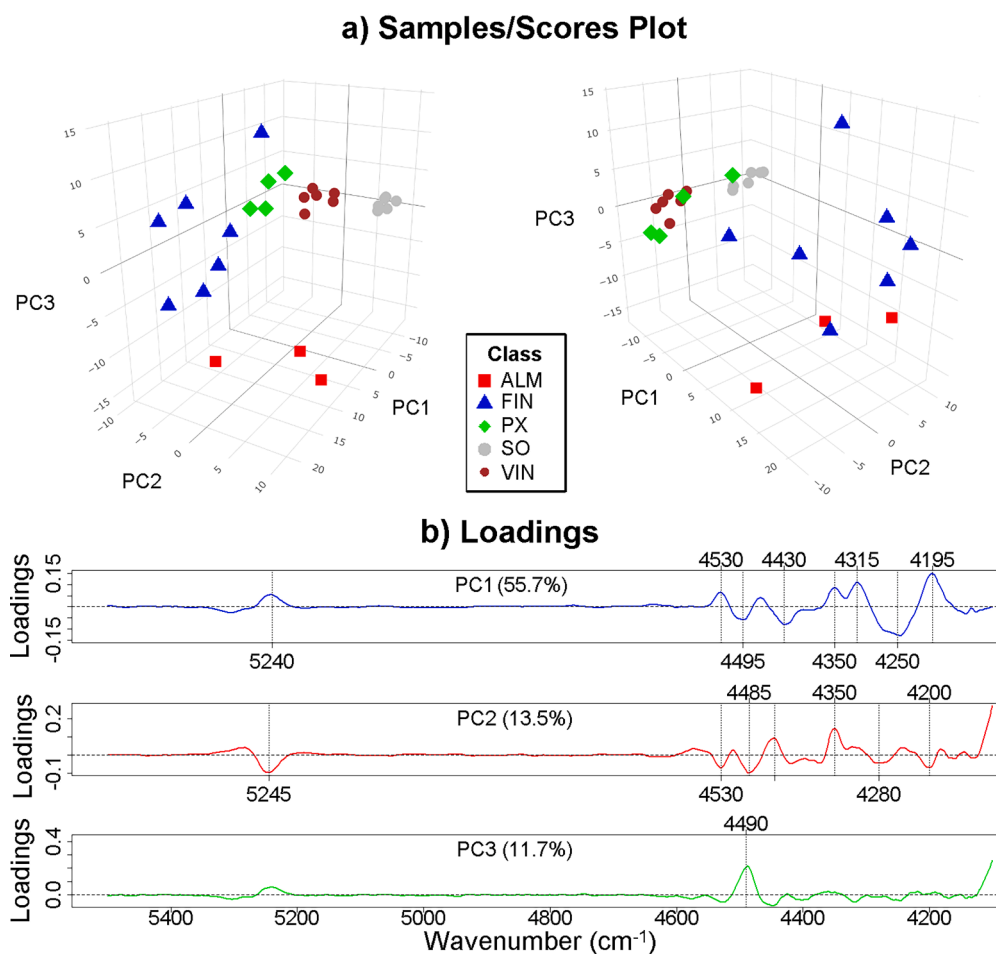

Fig. 5. PCA of FT-NIR spectroscopy results: samples/scores plots (a) and variable/loadings plot for PC1, PC2 and PC3 (b).

($\sim$4270 cm^{-1}). The presence of Mg can cause a shift of Al-OH band to lower wavenumbers in some clay minerals [54]. Concerning 4195 cm^{-1} loading peak, it is probably connected with 4190 cm^{-1} band that is more intense in PX, SO and VIN than in the other samples and could be related to the presence of amphiboles such as hornblende, especially since it is associated with 4310 cm^{-1} band [56]. It is worth noting that SO sample can be distinguished from VIN and PX ones on PC2, due to its high scores. One of the most intense loadings peaks is located at about 4350 cm^{-1}, which is positively correlated to this PC. It must be pointed out that VIN and PX spectra have a shoulder close to this wavenumber that, as previously stated, is linked to metal-OH vibrations. However, all the samples show a band around 4530 cm^{-1}, possibly caused by Al$_2$-OH vibrations in some clay minerals such as montmorillonite and kaolinite [57], and linked to loadings at $\sim$4530 cm^{-1}; at $\sim$4430 cm^{-1}, which is a metal-OH band present in several clay minerals like serpentines, chlorites and micas [54], probably linked also to the loadings at $\sim$4445 cm^{-1}; and between $\sim$4280 and $\sim$4250 cm^{-1}, which have a relevant influence in PC1 as well. The high PC3 scores of FIN compared to ALM are probably caused by the presence in the former of a well-resolved band at 4485 cm^{-1}, caused by metal-OH vibrations.

The groupings provided by the application of SOM on FT-NIR data could not clearly classify the sources of raw materials (see the Supplementary Online Materials: Annex 3b). Again, the small size of the sample together with the huge number of variables to be considered is making the mapping results difficult to interpret. Therefore, the size of sample should be increased to provide better classification through the SOM procedure.

4. Discussion of the analytical results

The dolerite samples from outcrops and the archaeological materials were characterised from the chemical point of view using three different techniques. While pED-XRF provides the concentrations of a set of elements present in the rocks, Raman and FT-NIR results are linked to their mineralogical phases. Thus, although elemental composition and mineralogy are tied one to each other, the three techniques do not offer necessarily the same information, since the same elements can be organised in different crystal structures that depend also on the petrogenetic conditions. Furthermore, alteration phenomena can lead to the formation of secondary minerals.

Several above-quoted studies based on pED-XRF showed that this technique suffers of limitations for many analytes in direct analysis of heterogeneous materials. Indeed, for most of them the measurement is limited to the very surface, which is problematic for easily mobilised elements due to weathering, while other elements, especially traces, are present at levels close or below to the limit of detection. Only four analytes (Rb, Sr, Zr and Ba) resulted reliable to discriminate among the potential sources and investigate the provenance of the archaeological materials. Relationships among Sr, Ba and Rb were chosen for classification. As can be observed in the scatter plot for log (Ba) vs log (Sr), and log (Rb) vs log (Sr) (Fig. 6a), some points fall close to ALM (S2, S4, S7) and some close to FIN and SO (S3, S6) samples or close to them. S1 and S5 fall among these three outcrops. Natural samples from ALT, PX and VIN are instead plotted far from the archaeological points.

Concerning Raman microspectroscopy, the characterisation of the bulk sample is quite problematic due to the very small measurement spot from the one hand, and to the dolerite complex mineralogical properties from the others. Though most of the spectral features could be assigned, the obtained spectra interpretation resulted very difficult because of the numerous characteristics and the presence of composite bands. The use of PCA was necessary to make interpretable such an amount of data. Scores for archaeological artefacts were predicted on the basis of PCA model of geological samples and cluster analysis was performed to observe grouping among the observations from the two classes (geological and archaeological, Fig. 6b). Artefacts points are closer to those from ALM and FIN samples than to the others. As previously stated, the most influential regions are those characterised by plagioclases and pyroxenes, whose spectral features are determined by the proportions among the metal cations [33,44] which could mark difference in original melt and petrogenetic conditions for these igneous
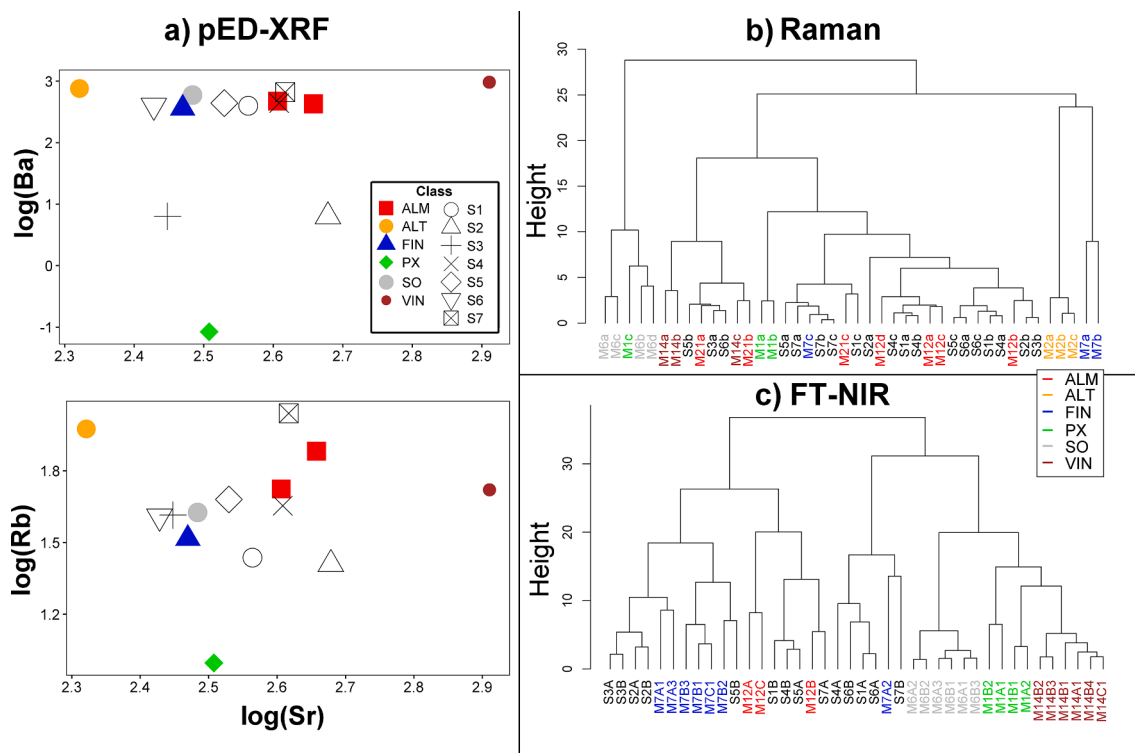

Fig. 6. Scatter plots of log-transformed mean concentration for Ba vs Sr and Rb vs Sr of artefacts and natural samples obtained by pED-XRF (a), and cluster analyses for PCA scores of Raman (b) and FT-NIR spectroscopy (c).

rocks. It should be pointed out that pED-XRF does not offer data on some of the metals present in pyroxenes and plagioclases (Na and Mg), while the amount of the other elements could be influenced also by the other minerals present in the rock. The fact that provenance hypothesis could have been improved by crossing Raman and pED-XRF is consistent with the complementary information provided by the two techniques.

The identification of the potential sources of raw materials was carried out by both FT-NIR spectroscopy and Raman. The obtained results are similar; indeed, according to cluster analysis (Fig. 6c), the stone tools have chemical features closer to ALM and FIN samples.

In conclusion, results from the three techniques are almost consistent within each other and indicate similar possible provenances. Furthermore, the complementary use of the different techniques suggests that FIN and ALM outcrops could have been the most probable sources for the raw material.

5. Conclusions

Interesting results concerning the identification of dolerite raw material provenance were obtained, successfully testing a non-invasive analytical approach.

Most of the archaeological stone tools show chemical features close to ALM, FIN and SO raw material samples. Multielement analysis seems to be less effective in discriminating among the different outcrops. It is possibly linked to the fact that only few analytes can be considered reliable for raw material identification due to the pED-XRF limitations. Raman microspectroscopy showed to be an effective complementary technique, giving information related to the mineralogical phases present in the samples, therefore supporting pED-XRF results. Indeed, SO outcrop could be ruled out as potential sources according to their mineralogy. The attribution suggested by multivariate statistics is mainly driven by the composition of dolerite essential minerals which are linked to the different petrogenetic conditions. FT-NIR results are similar to those of Raman and suggest ALM and FIN outcrops as the most likely sources of raw materials. However, on the contrary of pED-XRF and Raman microspectroscopy, FT-NIR evidenced certain differences between some spectra from archaeological and geological samples. Since FT-NIR is particularly sensitive to hydrous phases which in this lithotype can be found as secondary minerals, the conclusions inferred from this technique should be handed carefully, taking into account possible misleading results caused by the different alteration conditions of the samples.

CRediT authorship contribution statement

Mirco Ramacciotti: Formal analysis, Investigation, Data curation, Writing – original draft, Writing – review & editing, Visualization. **Gianni Gallello:** Conceptualization, Methodology, Formal analysis, Investigation, Data curation, Writing – original draft, Writing – review & editing, Visualization, Supervision, Project administration. **Joaquin Jiménez-Puerto:** Formal analysis, Investigation, Data curation, Writing – review & editing. **Joan Bernabeu:** Formal analysis, Investigation, Writing – original draft, Writing – review & editing, Visualization. **Teresa Orozco Köhler:** Resources, Writing – original draft, Writing – review & editing. **Sonia Rubio-Barberá:** Investigation. **Agustín Pastor:** Investigation, Writing – original draft, Writing – review & editing.

Declaration of Competing Interest

The authors declare that they have no known competing financial interests or personal relationships that could have appeared to influence the work reported in this paper.

Data availability

Data will be made available on request.

Appendix A. Supplementary data

Supplementary data to this article can be found online at https://doi.org/10.1016/j.microc.2022.108080.

References

[1] N. Forster, P. Grave, Non-destructive PXRF analysis of museum-curated obsidian from the Near East, J. Archaeol. Sci. 39 (2012) 728–736, https://doi.org/10.1016/j.jas.2011.11.004.

[2] A. Prieto, I. Yusta, A. Arrizabalaga, Defining and characterizing archaeological quartzite: Sedimentary and metamorphic processes in the lithic assemblages of El Habario and El Arteu (Cantabrian Mountains, Northern Spain), Archaeom. 61 (2019) 14–30, https://doi.org/10.1111/arcm.12397.

[3] A. Triantafyllou, N. Mattielli, S. Clerbois, A.C. Da Silva, P. Kaskes, P. Claeys, X. Devleeschouwer, G. Brkojewitsch, Optimizing multiple non-invasive techniques (PXRF, pMS, IA) to characterize coarse-grained igneous rocks used as building stones, J. Archaeol. Sci. 129 (2021), 105376, https://doi.org/10.1016/j.jas.2021.105376.

[4] S. Domínguez-Bella, J.M. Herrero, Archaeomineralogy of prehistoric artifacts and gemstones, in: J. Miguel Herrero, M. Vendrell (EdS.), International Seminar on Archaeometry and Cultural Heritage: the Contribution of Mineralogy (Bilbao, 27 de Junio 2012), Sociedad Española de Mineralogía, Madrid, 2012, pp. 5–28.

[5] M. Ramacciotti, G. Gallello, A. Pastor, A. Diez Castillo, O. García Puchol, Chert nucleus and cortex characterization for archaeological provenance study tested in the Prebaetic system region (Valencian community, Spain), Lithic Technol. 44 (2019) 166–180, https://doi.org/10.1080/01977261.2019.1618043.

[6] M. Ramacciotti, O. García-Puchol, A. Cortell-Nicolau, G. Gallello, Á. Morales-Rubio, A. Pastor, Moving to the land: First archaeometric study of chert procurement at Cueva de la Cocina (Eastern Iberia), Geoarchaeol. 37 (2022) 544–559, https://doi.org/10.1002/gea.21903.

[7] M. Ramacciotti, S. Rubio, G. Gallello, M. Lezzerini, S. Raneri, E. Hernandez, M. Calvo, S. Columbu, Á. Morales, A. Pastor, M. de la Guardia, Chemical and mineralogical analyses on stones from Sagunto Castle (Spain), J. Archaeol. Sci. Rep. 24 (2019) 931–938, https://doi.org/10.1016/j.jasrep.2019.03.017.

[8] S. Domínguez-Bella, D. Morata-Céspedes, Aplicación de las técnicas mineralógicas y petrológicas a la arqueometría. Estudio de Materiales de Alberite (Villamartín, Cádiz), Zephyrus XLVIII (1995) 129–142.

[9] C. Read, R. Grapes, K. Lillios, Petrography and chemical analyses of prehistoric amphibolite artefacts from Portugal and possible source rocks from Western Iberia, Anal. Facil. Publ. 19 (1997) 1–20.

[10] P. Santi, F. Antonelli, A. Renzulli, Provenance of Medieval pietra ollare artefacts found in archaeological sites of Central-Eastern Italy: insights into the Alpine soapstone trade, Archaeom. 47 (2005) 253–264, https://doi.org/10.1111/j.1475-4754.2005.00200.x.

[11] R.M. Parish, D.H. Werra, Characterizing "chocolate" flint using reflectance spectroscopy, Archaeol. Pol. 56 (2018) 89–101. https://doi.org/10.23858/APa56.2018.007.

[12] M.C. Jones, O. Williams-Thorpe, P.J. Potts, P.C. Webb, Using field-portable XRF to assess geochemical variations within and between dolerite outcrops of Preseli, South Wales, Geostand. Geoanal. Res. 29 (2005) 251–269, https://doi.org/10.1111/j.1751-908X.2005.tb00899.x.

[13] E. Frahm, R.C. Doonan, The technological versus methodological revolution of portable XRF in archaeology, J. Archaeol. Sci. 40 (2013) 1425–1434, https://doi.org/10.1016/j.jas.2012.10.013.

[14] R. Gill, Igneous rocks and processes: a practical guide, Wiley, Malaysia, 2011.

[15] M.J. Richards, Realising the potential of portable XRF for the geochemical classification of volcanic rock types, Optimizing multiple non-invasive techniques (PXRF, pMS, IA) to characterize coarse-grained igneous rocks used as building stones, J. Archaeol. Sci. 105 (2019) 31–45, https://doi.org/10.1016/j.jas.2019.03.004.

[16] O. Williams-Thorpe, P.C. Webb, M.C. Jones, Non-destructive geochemical and magnetic characterisation of Group XVIII dolerite stone axes and shaft-hole implements from England, J. Archaeol. 30 (2003) 1237–1267, https://doi.org/10.1016/S0305-4403(02)00274-1.

[17] P. Grave, V. Attenbrow, L. Sutherland, R. Pogson, N. Forster, Non-destructive pXRF of mafic stone tools, J. Archaeol. Sci. 39 (2012) 1674–1686, https://doi.org/10.1016/j.jas.2011.11.011.

[18] M. Wojcieszak, L. Wadley, Raman spectroscopy and scanning electron microscopy confirm ochre residues on 71,000-year-old bifacial tools from Sibudu, South Africa, *Archaeom* 60 (2018) 1062–1076, https://doi.org/10.1111/arcm.12369.

[19] O. Williams-Thorpe, P.J. Potts, P.C. Webb, Field-portable non-destructive analysis of lithic archaeological samples by X-ray fluorescence instrumentation using a mercury iodide detector: comparison with wavelength-dispersive XRF and a case study in British stone axe provenancing, J. Archaeol. Sci. 26 (1999) 215–237, https://doi.org/10.1006/jasc.1998.0323.

[20] O. Williams-Thorpe, M.C. Jones, P.J. Potts, P.C. Webb, Preseli dolerite bluestones: Axe-heads, Stonehenge monoliths, and outcrop sources, Oxf. J. Archaeol. 25 (2006) 29–46, https://doi.org/10.1111/j.1468-0092.2006.00247.x.

[21] R.E. Bevins, N.J. Pearce, R.A. Ixer, Revisiting the provenance of the Stonehenge bluestones: Refining the provenance of the Group 2 non-spotted dolerites using rare earth element geochemistry, J. Archaeol. Sci. Rep. 38 (2021), 103083, https://doi.org/10.1016/j.jasrep.2021.103083.

[22] T. Orozco-Köhler, Aprovisionamiento e Intercambio: Análisis petrológico del utillaje pulimentado en la Prehistoria Reciente del País Valenciano (España), BAR Publishing, Oxford, 2000.

[23] G. Gallello, T. Orozco, A. Pastor, M. de la Guardia, J. Bernabeu, Regional provenance of dolerite prehistoric objects through mineral análisis, Microchem. J. 124 (2016) 167–174, https://doi.org/10.1016/j.microc.2015.08.018.

[24] T. Orozco Köhler, G. Gallello, Testing a new methodological approach to define the use of dolerite outcrops for prehistoric tool production in Mediterranean Iberia, in: T. Pereira, X. Terradas, N. Bicho (Eds.), Raw Materials Exploitation in Prehistory: Sourcing, Processing and Distribution, Cambridge Scholars Publishing, Newcastle upon Tyne, 2017, pp. 193–205.

[25] R Core Team, R: A language and environment for statistical computing. R Foundation for Statistical Computing, 2021, Wien, Austria.

[26] T. Kohonen, Self-organized formation of topologically correct feature maps, Biol. Cybern. 43 (1) (1982) 59–69, https://doi.org/10.1007/BF00337288.

[27] J. Zupan, J. Gasteiger, Neural networks in chemistry and drug design: an Introduction, 2nd ed., Wiley, Weinheim, Germany, 1999.

[28] A. Astel, S. Tsakovski, P. Barbieri, V. Simeonov, Comparison of self-organizing maps classification approach with cluster and principal components analysis for large environmental data sets, Water Res. 41 (19) (2007) 4566–4578, https://doi.org/10.1016/j.watres.2007.06.030.

[29] H. Wickham, ggplot2: Elegant Graphics for Data Analysis, Springer, New York, 2016. https://doi.org/10.1007/978-0-387-98141-3.

[30] C. Sievert, Interactive Web-Based Data Visualization with R, plotly, and shiny, Chapman and Hall/CRC Press, Boca Raton, Florida, 2020.

[31] R. Wehrens, J. Kruisselbrink, Flexible self-organizing maps in kohonen 3.0, J. Stat. Softw. 87 (7) (2018) 1–18. https://doi.org/10.18637/jss.v087.i07.

[32] P.J. Potts, F. Bernardini, M.C. Jones, O. Williams-Thorpe, P.C. Webb, Effects of weathering on in situ portable X-ray fluorescence analyses of geological outcrops: dolerite and rhyolite outcrops from the Preseli Mountains, South Wales, X-Ray Spectrom. 35 (2006) 8–18, https://doi.org/10.1002/xrs.881.

[33] D. Ogburn, B. Sillar, J.C. Sierra, Evaluating effects of chemical weathering and surface contamination on the in situ provenance analysis of building stones in the Cuzco region of Peru with portable XRF, J. Archaeol. Sci. 40 (2013) 1823–1837, https://doi.org/10.1016/j.jas.2012.09.023.

[34] M.C. Jones, O. Williams-Thorpe, An illustration of the use of an atypicality index in provenancing British stone axes, Archaeom. 43 (2001) 1–18, https://doi.org/10.1111/j.1475-4754.2001.00001.x.

[35] E. Huang, C.H. Chen, T. Huang, E.H. Lin, J.A. Xu, Raman spectroscopic characteristics of Mg-Fe-Ca pyroxenes, Am. Mineral. 85 (2000) 473–479, https://doi.org/10.2138/am-2000-0408.

[36] G. Berlanga, T.E. Acosta-Maeda, S.K. Sharma, J.N. Porter, P. Dera, H. Shelton, G. J. Taylor, A.K. Misra, Remote Raman spectroscopy of natural rocks, Appl. Opt. 58 (2019) 8971–8980, https://doi.org/10.1364/AO.58.008971.

[37] K.E. Kuebler, B.L. Jolliff, A. Wang, L.A. Haskin, Extracting olivine (Fo–Fa) compositions from Raman spectral peak positions, Geochim. Cosmochim. Acta 70 (2006) 6201–6222, https://doi.org/10.1016/j.gca.2006.07.035.

[38] J.T. Kloprogge, Raman spectroscopy of clay minerals, in: W.P. Gates, J. T. Kloprogge, F. Madejová, F. Bergaya (Eds.), Developments in Clay Science, vol. 8, Elsevier, 2017, pp. 150–199, https://doi.org/10.1016/B978-0-08-100355-8.00006-0.

[39] N. Buzgar, A.I. Apopei, V. Diaconu, A. Buzatu, The composition and source of the raw material of two stone axes of Late Bronze Age from Neamt County (Romania)-A Raman study, Analele Stiintifice de Universitatii AI Cuza din Iasi. Sect. 2, Geologie 59 (2013) 5–22.

[40] T.P. Mernagh, A.G. Trudu, A laser Raman microprobe study of some geologically important sulphide minerals, Chem. Geol. 103 (1993) 113–127, https://doi.org/10.1016/0009-2541(93)90295-T.

[41] S. Andò, E. Garzanti, Raman spectroscopy in heavy-mineral studies, Geol. Soc., London, Spec. Publ. 386 (2014) 395–412, https://doi.org/10.1144/SP386.2.

[42] R. Stalder, A. Kronz, B.C. Schmidt, Raman spectroscopy of synthetic (Mg, Fe) SiO$_3$ single crystals. An analytical tool for natural orthopyroxenes, Eur. J. Mineral. 21 (1) (2009) 27–32.

[43] D.W. Matson, S.K. Sharma, J.A. Philpotts, Raman spectra of some tectosilicates and of glasses along the orthoclase-anorthite and nepheline-anorthite joins, Am. Mineral. 71 (1986) 694–704.

[44] K.D. Litasov, N.M. Podgornykh, Raman spectroscopy of various phosphate minerals and occurrence of tuite in the Elga IIE iron meteorite, J. Raman Spectrosc. 48 (2017) 1518–1527, https://doi.org/10.1002/jrs.5119.

[45] Z.C. Ling, A. Wang, B.L. Jolliff, Mineralogy and geochemistry of four lunar soils by laser-Raman study, Icarus 211 (2011) 101–113, https://doi.org/10.1016/j.icarus.2010.08.020.

[46] J.J. Freeman, A. Wang, K.E. Kuebler, B.L. Jolliff, L.A. Haskin, Characterization of natural feldspars by Raman spectroscopy for future planetary exploration, Can. Mineral. 46(6) (2008) 1477–1500. https://doi.org/ 10.3749/canmin.46.6.1477.

[47] O.N. Shebanova, P. Lazor, Raman spectroscopic study of magnetite (FeFe$_2$O$_4$): a new assignment for the vibrational spectrum, J. Solid State Chem. 174 (2003) 424–430, https://doi.org/10.1016/S0022-4596(03)00294-9.

[48] A. Buzatu, N. Buzgar, 2010. The Raman study of single-chain silicates. Analele Stiintifice de Universitatii AI Cuza din Iasi. Sect. 2, Geologie 56, 107125. https://doi.org/10.13140/2.1.4600.9288.

[49] A. Wang, J.J. Freeman, B.L. Jolliff, Understanding the Raman spectral features of phyllosilicates, J. Raman Spectrosc. 46 (2015) 829–845, https://doi.org/10.1002/jrs.4680.

[50] S.K. Sharma, S.M. Angel, M. Ghosh, H.W. Hubble, P.G. Lucey, Remote pulsed laser Raman spectroscopy system for mineral analysis on planetary surfaces to 66 meters, Appl. Spectrosc. 56 (2002) 699–705, https://doi.org/10.1366/000370202760077630.

[51] D.C. Smith, F. Gendron, Archaeometric application of the raman microprobe to the non-destructive identification of the two pre-columbian ceremonial polished 'greenstone' axe-heads from mesoamerica, J. Raman Spectrosc. 28 (1997) 731–738, https://doi.org/10.1002/(sici)1097-4555(199709)28:93.0.co;2-9.

[52] N. Buzgar, A.I. Apopei, The Raman study of certain carbonates, Geol. Tomul L 2 (2009) 97–112. https://doi.org/10.13140/2.1.1358.3368.

[53] R.N. Clark, T.V. King, M. Klejwa, G.A. Swayze, N. Vergo, High spectral resolution reflectance spectroscopy of minerals, J. Geophys. Res. Solid Earth 95 (1990) 12653–12680, https://doi.org/10.1029/JB095iB08p12653.

[54] J. Bishop (2019). Visible and Near-Infrared Reflectance Spectroscopy: Laboratory Spectra of Geologic Materials, in: J. Bishop, J. Bell III, J. Moersch (Eds.), Remote Compositional Analysis: Techniques for Understanding Spectroscopy, Mineralogy, and Geochemistry of Planetary Surfaces, Cambridge University Press, Cambridge, 2019, pp. 68–101. https://doi.org/10.1017/9781316888872.006.

[55] A.R. Philpotts, Petrography of Igneous and Metamorphic Rocks, Waveland Press, Prospect Height, Illinois, USA, 1989.

[56] M. Kokkaliari, I. Iliopoulos, Application of Near-Infrared Spectroscopy for the identification of rock mineralogy from Kos Island, Aegean Sea, Greece, Bull. Geol. Soc. Greece 55 (1) (2019) 290–308. https://doi.org/10.12681/bgsg.20708.

[57] J.L. Bishop, M.D. Lane, M.D. Dyar, A.J. Brown, Reflectance and emission spectroscopy study of four groups of phyllosilicates: smectites, kaolinite-serpentines, chlorites and micas, Clay Miner. 43 (2008) 35–54, https://doi.org/10.1180/claymin.2008.043.1.03.